



## Dual-damage constitutive model to define thermal damage in rock

Liyuan Liu<sup>a,\*</sup>, Hongguang Ji<sup>a,\*\*</sup>, Derek Elsworth<sup>b</sup>, Sheng Zhi<sup>b</sup>, Xiangfeng Lv<sup>a</sup>, Tao Wang<sup>a</sup>

<sup>a</sup> Beijing Key Laboratory of Urban Underground Space Engineering, School of Civil and Resource Engineering, University of Science and Technology Beijing, Beijing, 100083, China

<sup>b</sup> Department of Energy and Mineral Engineering, EMS Energy Institute and G3 Center, Pennsylvania State University, University Park, PA, 16802, USA

### ARTICLE INFO

#### Keywords:

Thermal-mechanical coupling  
Dual-damage constitutive model  
Thermal damage  
Porosity and permeability  
Strength  
Tensile damage

### ABSTRACT

The evolution of the mechanical properties of rock as a function of thermal damage is relevant to various engineering applications, such as nuclear waste repositories, underground coal gasification, dry-fracture shale system and geothermal energy extraction. The thermal properties of heterogeneous rock control heat transmission with differential thermal expansion potentially resulting in significant changes in the mechanical and transport behavior of reservoir rocks. We define a novel dual-damage thermal-mechanical model accommodating the interaction of thermal conductivity, thermally-induced deformation, rock mechanical deformation and damage to define the evolution of the thermal and mechanical properties of rock during thermal treatment. Importantly, the dual-damage constitutive model is capable of using elastic modulus and strength to solve for asynchronous changes in peak strain and peak strength, respectively. The proposed model is validated against analytical solutions and laboratory data. The results indicate that thermally-induced damage increases rock porosity and permeability while simultaneously decreasing elastic modulus and strength. Thermal treatment causes a realignment in the rock microstructure and results in a change in the ultimate failure pattern. Thermally-induced damage causes irreversible increases in rock porosity and permeability even as temperature is restored. Furthermore, it is confirmed that thermally-induced damage in rock is dominated by the type of tensile damage during the thermal expansion. The proposed dual-damage constitutive model better explains the non-proportional relationship between peak strength and peak strain observed in many experiments.

### 1. Introduction

Thermally-induced damage in rock plays a vital role in various engineering applications, including containment in nuclear waste repositories, underground coal gasification, dry-fracture shale system, geothermal energy extraction, and deep mining.<sup>1–5</sup> Therefore, it is of significance to understand the changes in rock mechanical properties induced by thermal damage for the design and for safety assessment in deep underground rock engineering.

Rocks can be considered as a typical dual porosity media, containing ‘solid’ space (i.e., the mineral matrix) and ‘void’ space (the sets of cracks and pores). The mechanical strength of rocks depends strongly on the geometry and density of the cracks and pores.<sup>6,7</sup> Furthermore, the crack and pore structure of rock are closely related to thermal treatment. When temperatures are elevated, the micro-structure of the rock mass may change during thermal expansion, including the growth of new micro-cracks, extension and/or widening of the existing micro-cracks

together with various mineralogical alterations.<sup>8</sup> Simultaneously, rock stress-strain relationships and failure criteria change with temperature. As a result, many rock mechanical properties, such as compressive strength, tensile strength, elastic modulus, cohesive strength and friction angle decrease with an increase in temperature.<sup>9–11</sup>

Many experimental investigations have been conducted in an attempt to further understand the evolution of rock mechanical behaviors when subjected to elevated temperatures.<sup>12–15</sup> Experimental studies on the stress-strain response of granite at various temperatures demonstrate that the compressive strength and elastic modulus of granites decreases as temperature increases.<sup>10,16,17</sup> High temperature has a significant effect on porosity evolution<sup>14</sup> with porosity generally increasing with increased temperature. The effects of thermally and mechanically activated dissolution of minerals impact the mechanical and transport response of fractured rock<sup>18</sup> and these effects become dominant high temperature. Microscopic investigations indicate that damage in rocks at elevated temperatures is induced to different degrees

\* Corresponding author.

\*\* Corresponding author.

E-mail addresses: [liuliyuan@ustb.edu.cn](mailto:liuliyuan@ustb.edu.cn) (L. Liu), [jihongguang@ces.ustb.edu.cn](mailto:jihongguang@ces.ustb.edu.cn) (H. Ji).

<https://doi.org/10.1016/j.ijrmmms.2019.104185>

Received 13 August 2019; Received in revised form 18 October 2019; Accepted 18 December 2019

Available online 21 December 2019

1365-1609/© 2019 Elsevier Ltd. All rights reserved.

of severity depending on grain size, porosity, and structural and textural characteristics.<sup>7</sup> High temperature induces irreversible changes in the rock properties.<sup>19,20</sup>

Many numerical simulations on thermal-induced rock damage are also studied. Hueckel et al<sup>21</sup> proposed a constitutive model proposed for thermo-plastic behavior of rock based on a macroscopic modeling approach, in which the empirical dependence of its constitutive functions on temperature is used to describe thermal effects rather than rock specific microscale mechanism. Tang et al<sup>22–24</sup> and Li et al<sup>25</sup> developed a series of coupled thermo-mechanical-damage models in RFPA to examine rock failure processes induced by thermal stress. Although some experimental phenomena can be explained by these models, they all assume that the elastic modulus and strength of rock obey the same damage law, and the non-proportional alteration of elastic modulus and strength of rock observed in many experiments cannot be verified properly. The experimental observations cannot be satisfactorily explained by either mechanical or numerical models. In particular, the mechanism of non-proportional alteration of peak strain and peak strength observed in various experiments are not revealed through theoretical models.

The understanding of the behavior of altered rocks requires an accurate geomechanical model, in which the evolution of important physical and mechanical characteristics has to be included. This work provides a detailed description of the evolution of rock alteration during different thermal treatments. We develop a novel thermal-mechanical coupled model based on dual damage constitutive theory, to simulate the rock mechanical behaviors induced by thermal damage. The proposed model is validated by analytical solutions and laboratory data.

## 2. Dual-damage constitutive model

Routine theory cannot accommodate the effect of ductility of a material upon the thermal stresses which can be induced therein. This is because routine theory assumes that the thermal conductivity, thermal expansion, elastic modulus, Poisson's ratio, strength, porosity, and permeability are all constant. The following defines a method that allows all these co-called constants to evolve with the temperature path and, more importantly, may accommodate stress-strain curves which respond to damage, as illustrated in Fig. 1.

When rocks are exposed to high temperatures, the complex interaction of stress and thermal-induced damage exert a strong influence on properties. These include influences on thermal transport, rock deformation via porosity and permeability, thermal conductivity and thereby spatial heat change. In this study, we define this chain of reactions as “coupled processes” implying that one physical or mechanical process affects the initiation and evolution of another. In particular, damage is at

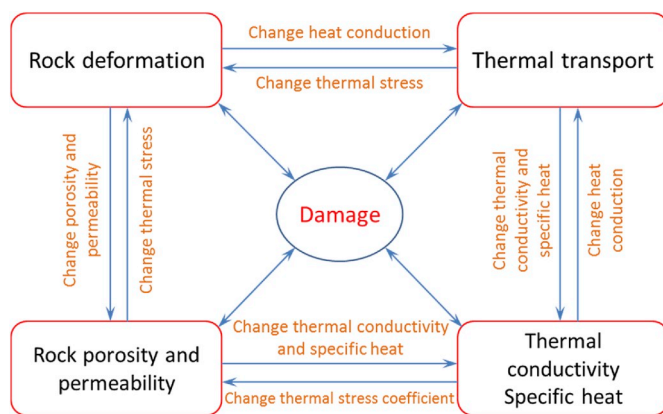


Fig. 1. Interactions of multiple coupled processes through a thermal-stress-controlled rock porosity model and rock permeability model defined as a function of the damage during thermal treatment.

the core of interactions of multiple coupled processes. Therefore, the inclusion of damage is the key to rigorously formulate the full mechanics of thermal-mechanical-damage (TMD) coupling interactions. Furthermore, the damage model in this study is based on a novel dual-damage constitutive theory. The thermal analysis provides interactive coupling to mechanical stress calculations through the thermal expansion coefficient and damage evolution law. Thermal volumetric strain and dual-damage constitutive models are introduced into the incremental mechanical constitutive laws to account for the TMD coupling.

### 2.1. Governing equation for heat conduction

The general formulation for heat conduction through rock is given by:

$$\lambda \nabla^2 T + Q = \rho C \frac{\partial T}{\partial t} \quad (1)$$

Where  $\lambda$  is thermal conductivity,  $Q$  is the source term,  $\rho$  is the equivalent density,  $C$  is the specific heat capacity, and  $t$  is the time.

### 2.2. Constitutive models for rock porosity and permeability

Rock porosity is related to the effective strain of the pores and fractures as<sup>26</sup>:

$$\frac{\varphi}{\varphi_0} = 1 + \frac{1}{\varphi_0} \Delta \varepsilon_e \quad (2)$$

where  $\varphi_0$  is the initial rock porosity,  $\varphi$  is the current rock porosity, and  $\Delta \varepsilon_e$  is the increment of effective strain.

In this study, only the increment of effective strain  $\Delta \varepsilon_e$  is responsible for the rock porosity and permeability change. The effective strain is the resultant of the total volumetric strain and the thermal strain. The change in the effective strain is:

$$\Delta \varepsilon_e = \Delta \varepsilon_v - \alpha_T \Delta T \quad (3)$$

where  $\Delta \varepsilon_v$  is the total volumetric strain,  $\alpha_T \Delta T$  is the thermal strain,  $\alpha_T$  is thermal expansion coefficient ( $^{\circ}\text{C}^{-1}$ ), and  $\Delta T$  is the temperature change.

According to the typical cubic relationship between permeability and porosity,<sup>27,28</sup> we obtain permeability model:

$$\frac{k}{k_0} = \left[ 1 + \frac{1}{\varphi_0} (\Delta \varepsilon_v - \alpha_T \Delta T) \right]^3 \quad (4)$$

### 2.3. Governing equation for mechanical response

For static equilibrium of the medium, mechanical equilibrium of the solid phase is defined as:

$$\sigma_{ij,j} - f_i = 0 \quad (5)$$

where  $\sigma_{ij,j}$  represents the divergence of the transpose of the Cauchy stress tensor and  $f_i$  is the body force per unit volume.

The constitutive equation (Hooke's Law) defines the relation between the total bulk stress components,  $\sigma_{ij}$ , and strain components,  $\varepsilon_{ij}$ , when the temperature change  $T$  is also included. The stress-strain law is given by:

$$\sigma_{ij} = 2G\varepsilon_{ij} + \frac{2G\nu}{1-2\nu} \varepsilon_{kk} \delta_{ij} - \frac{2G(1+\nu)}{1-2\nu} \alpha_T T \delta_{ij} \quad (6)$$

where  $G$  is the equivalent shear modulus of the rock,  $\nu$  is Poisson's ratio,  $\delta_{ij}$  is the Kronecker delta defined as 1 for  $i=j$  and 0 for  $i \neq j$ ,  $\alpha_T$  is coefficient of thermal expansion ( $^{\circ}\text{C}^{-1}$ ), and the linearized strains are defined as the symmetric part of the displacement gradient  $u_{ij}$ ,

$$\varepsilon_{ij} = \frac{1}{2} (u_{i,j} + u_{j,i}) \quad (7)$$

Substituting Eq. (7) into Eq. (6) and the result into the static equilibrium equation, Eq. (9), yields the Navier equation for the displacements,

$$Gu_{i,kk} + \frac{G}{1-2\nu}u_{k,ki} - \frac{2G(1+\nu)}{1-2\nu}\alpha_T T_{,i} + f_i = 0 \quad (8)$$

where Eq. (8) is the governing equation for rock deformation under the influence of the temperature change.

#### 2.4. Constitutive model accommodating heterogeneity and dual-damage evolution

A realistic analysis of the coupled thermal-mechanical response must rely on numerical modeling with adequate consideration of heterogeneities.<sup>24,29</sup> Microstructural variables have a significant effect on the evolution of rock damage.<sup>30,31</sup> To characterize heterogeneity at the mesoscopic-level, mechanical parameters such as elastic modulus, strength, Poisson's ratio, and thermal expansion coefficient may be assigned according to the Weibull distribution.<sup>32,33</sup> This distribution defines parameters according to a probability density function as:

$$f(u) = \frac{m}{u_0} \left(\frac{u}{u_0}\right)^{m-1} e^{-\left(\frac{u}{u_0}\right)^m} \quad (9)$$

where  $u$  is the parameter of interest (such as elastic modulus or strength); the scale parameter  $u_0$  is related to the average of the element parameter, and  $m$  is the shape parameter of the Weibull distribution function. The parameter  $m$  is defined as the degree of material homogeneity and called the homogeneity index.

According to Eq. (9), we obtain the distribution of rock elastic modulus for the homogeneity index specified as 10, as shown in Fig. 2. As can be seen from Fig. 2 (a), the spatial distribution of rock elastic modulus is random. Fig. 2 (b) shows the probability density of the rock elastic modulus calculated by Eq. (9).

As illustrated in Fig. 3, rock damage in tension or shear is initiated when its state of stress (positive for compression) satisfies the maximum tensile stress criterion or the Mohr-Coulomb criterion, respectively<sup>32,34</sup> as:

$$F_1 = -\sigma_3 - f_{t0} = 0, \quad F_2 = \sigma_1 - \sigma_3 \frac{1 + \sin \theta}{1 - \sin \theta} - f_{c0} = 0 \quad (10)$$

where  $f_{t0}$  and  $f_{c0}$  are uniaxial tensile and compressive strength (Pa), respectively,  $\sigma_1$  and  $\sigma_3$  are major and minor principal stresses (Pa), respectively,  $\theta$  is internal frictional angle ( $^\circ$ ), and  $F_1$  and  $F_2$  are two

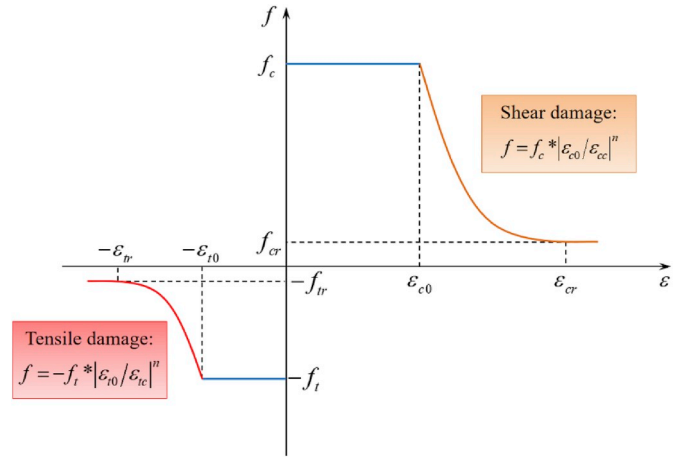


Fig. 3. Elastic damage-based constitutive law for strength ( $f_{t0}$  and  $f_{c0}$  are uniaxial tensile strength and uniaxial compressive strength, respectively).

damage threshold functions (Pa).

According to Fig. 3, the damage variable for the rock strength can be calculated as:

$$D_s = \begin{cases} 0 & F_1 < 0 \text{ and } F_2 < 0 \\ 1 - \left|\frac{\varepsilon_{t0}}{\varepsilon_3}\right|^n & F_1 = 0 \text{ and } dF_1 > 0 \\ 1 - \left|\frac{\varepsilon_{c0}}{\varepsilon_1}\right|^n & F_2 = 0 \text{ and } dF_2 > 0 \end{cases} \quad (11)$$

where  $\varepsilon_1$  and  $\varepsilon_3$  are the major and minor principal strains, respectively.  $\varepsilon_{t0}$  and  $\varepsilon_{c0}$  are the maximum tensile and maximum compressive principal strains when tensile and shear damage occurs, respectively.  $D_s$  represents the damage variable of rock strength and  $n$  is a constitutive coefficient for rock strength. In this study, the element, as well as its damage, is assumed isotropic, so the  $D_s$  and  $n$  parameters are all scalars.

As shown in Fig. 4, based on the theory of elastic damage, the elastic modulus of the damaged rock is expressed as:

$$E = E_0(1 - D_c) = \begin{cases} E_0 & F_1 < 0 \text{ and } F_2 < 0 \\ E_0 * \left|\frac{\varepsilon_{t0}}{\varepsilon_3}\right|^l & F_1 = 0 \text{ and } dF_1 > 0 \\ E_0 * \left|\frac{\varepsilon_{c0}}{\varepsilon_1}\right|^l & F_2 = 0 \text{ and } dF_2 > 0 \end{cases} \quad (12)$$

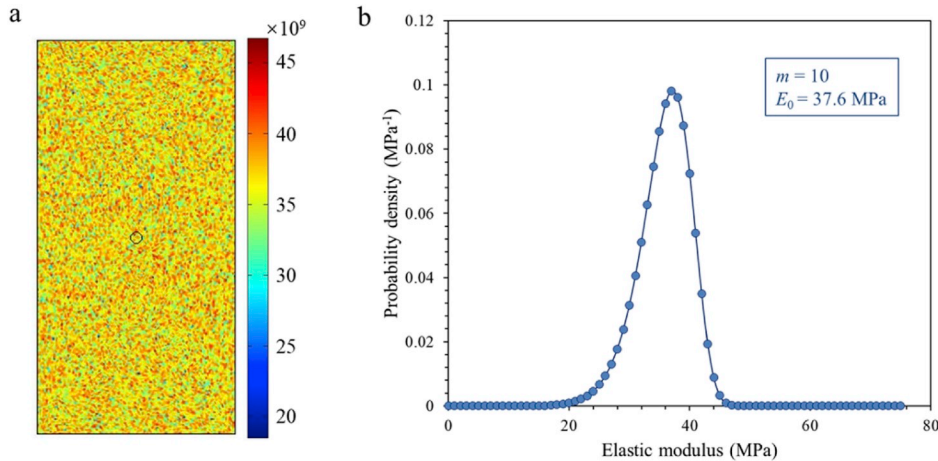


Fig. 2. Distributions of rock elastic modulus with the homogeneity index specified as 10. (a) Spatial distribution of rock elastic modulus, (b) Probability density of rock elastic modulus.

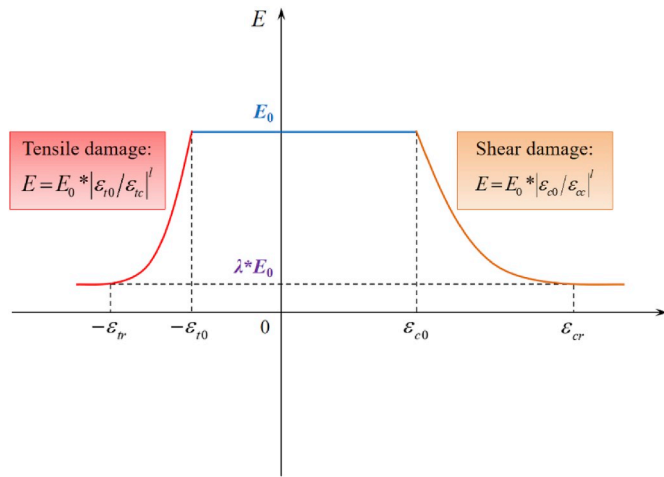


Fig. 4. Elastic damage-based constitutive law for elastic modulus ( $\lambda$  represents coefficient of residual strength).

where  $D_e$  represents the damage variable applied to the elastic modulus,  $l$  is a constitutive coefficient for the elastic modulus, and  $E$  and  $E_0$  are the elastic modulus (Pa) of the damaged and the undamaged rock, respectively. Similarly, rock is assumed isotropic, so the  $E$ ,  $E_0$ ,  $D_e$ , and  $l$  parameters are all scalars.

Under any stress and initial conditions, the tensile stress criterion is applied sequentially. In other words, the maximum tensile stress criterion is first applied to judge whether the elements are first damaged in tension or not. Only elements that survive this test will be checked for damage in shear using the Mohr-Coulomb criterion. In Eqs. (11) and (12), when  $F_1 < 0$  and  $F_2 < 0$  the applied stress is insufficient to satisfy the maximum tensile stress criterion and the Mohr-Coulomb failure criterion, respectively.  $F_1 = 0$  and  $dF_1 > 0$  implies rock damage in tensile mode when the stress state satisfies the maximum tensile stress criterion and the rock is still under load.  $F_2 = 0$  and  $dF_2 > 0$  implies rock damage in shear mode when the stress state satisfies the Mohr-Coulomb failure criterion and the rock remains loaded.

Considering the irreversibility of rock damage, the damage variable may only increment monotonically from zero during loading ( $dF_1 > 0$  or  $dF_2 > 0$ ) and remain unchanged during unloading ( $dF_1 < 0$  or  $dF_2 < 0$ ). In this respect, the damage defined by Eq. (11), reduces the strength of the rock. The damage calculated by Eq. (12), reduces the elastic modulus  $E$  and the shear modulus  $G$  of the rock. Since the dual-damage constitutive model is nonlinear both in space and time, the complete set of coupled equations is solved by numerical method. In addition, the damage variable and the damage-induced alterations of elastic modulus, strength, permeability, and other thermal properties are continually updated as the temperature and load increase. The basic implementation procedure is shown in Fig. 5.

### 2.5. Constitutive model for thermal properties evolution with damage

Many observations suggest that the thermal properties of rock are not constant, but vary with temperature or loading, particularly when damage or cracking occurring. During the loading process a significant number of open (air-filled) cracks may develop. In principle, their effects can be evaluated, in the macroscopic sense, by the use of mixing rules to take into account the air-filled volume fraction in the rock sample.

The temperature dependence of thermal conductivity may be empirically expressed as<sup>35</sup>:

$$\lambda(T) = \frac{\lambda(T_0)}{0.99 + (a - b/\lambda(T_0))(T - 273.15)} \quad (13)$$

with empirical constants and corresponding uncertainties  $a = 0.0030 \pm$

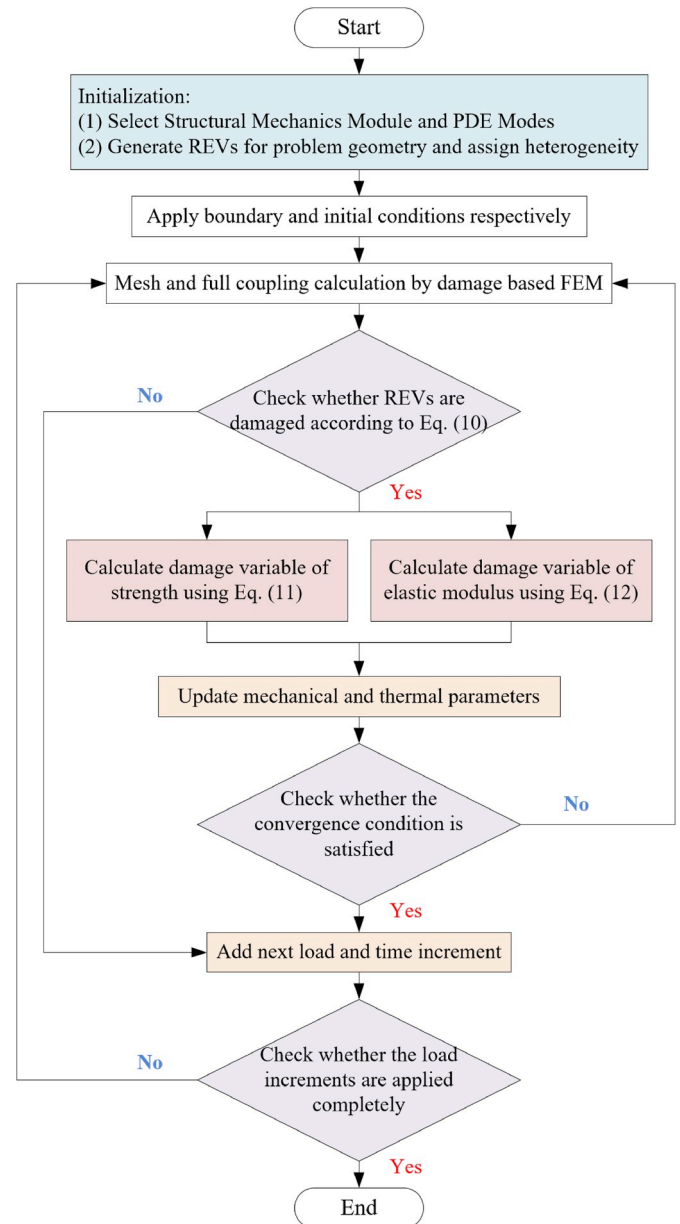


Fig. 5. Numerical implementation procedure of the dual-damage constitutive model.

0.0015 and  $b = 0.0042 \pm 0.0006$  representing crystalline rocks. The constants for corresponding sedimentary rocks are  $a = 0.0034 \pm 0.0006$  and  $b = 0.0039 \pm 0.0014$ .  $\lambda$  is given in  $Wm^{-1}$ ,  $T$  in K.

In thermal-mechanical damage model, a coefficient  $\xi_1$  is introduced to reflect the decrease in thermal conductivity induced by element failure by incorporating an air filled crack. The variation in the thermal conductivity of the mesoscopic element is thus assumed to be formulated as:

$$\lambda(T) = \begin{cases} \frac{\lambda(T_0)}{0.99 + (a - b/\lambda(T_0))(T - 273.15)} & D < 1 \\ \xi_1 \lambda(T_0) & D = 1 \end{cases} \quad (14)$$

where  $\xi_1$  is the damage factor with respect to thermal conductivity, which reflects the change of thermal conductivity induced by damage, based on the ratio of thermal conductivity of rock and air, commonly specified as  $\sim 0.01$ .

Experimental studies have shown that the effect of the temperature

on specific heat is also large and should be accounted for. The specific heat capacity at constant pressure is a function of temperature.<sup>24,36</sup> Therefore, the evolution of the specific heat of the mesoscopic element is assumed to be expressed as:

$$C_T(T) = \begin{cases} C_0(1 + \psi T) & D < 1 \\ \xi_1 C_0 & D = 1 \end{cases} \quad (15)$$

where  $C_0$  is the initial specific heat capacity of the intact rock mesoscopic element,  $\psi$  is an impact factor, which is assigned to  $3 \times 10^{-3} \text{ } ^\circ\text{C}^{-1}$  according to experimental results, and  $\xi_2$  is the damage factor applying to the specific heat, which reflects the change in the specific heat capacity induced by thermal damage. Similar to the damage factor for thermal conductivity,  $\xi_2$  is based on the ratio of the specific heat capacities of rock and air, and commonly specified as  $\sim 1.6$ .

### 3. Model validation

The proposed dual-damage constitutive theory TMD model is validated against analytical solutions and experimental observations. First, the proposed TMD model is validated against analytical solutions, in which the distribution of the temperature and stress fields are individually verified. Especially, since the analytical solution is a completely elastic solution, the model solution calculated by FEM code does not consider the effect of damage. Second, the proposed TMD model is compared with experimental observations of stress-strain curves and porosity evolution.

#### 3.1. Validation against analytical solutions

The analytical study is carried out considering a cylindrical core embedded in a rock cylinder, as shown in Fig. 6. The temperature distribution in a concentric thick-walled cylinder is expressed as:

$$T(\rho) = \frac{T_a \ln(b/\rho) + T_b \ln(\rho/a)}{\ln(b/a)} \quad (16)$$

where  $a$  is the radius of the core and  $b$  is the radius of rock cylinder,  $T_a$  is temperature of the core and  $T_b$  is temperature of the rock cylinder.

Due to the temperature increase, a radial pressure  $p$  will be induced in the rock surrounding the core.<sup>37,38</sup> According to the plane stress

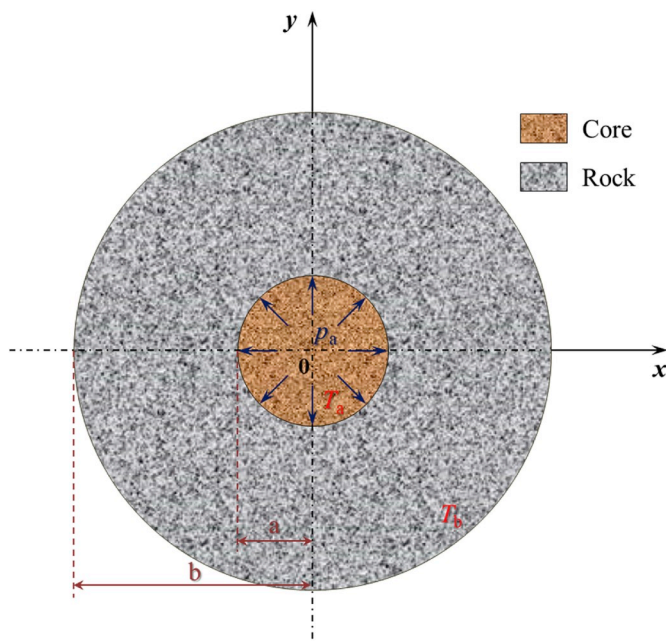


Fig. 6. Axisymmetric model of a solid core embedded in a rock anulus.

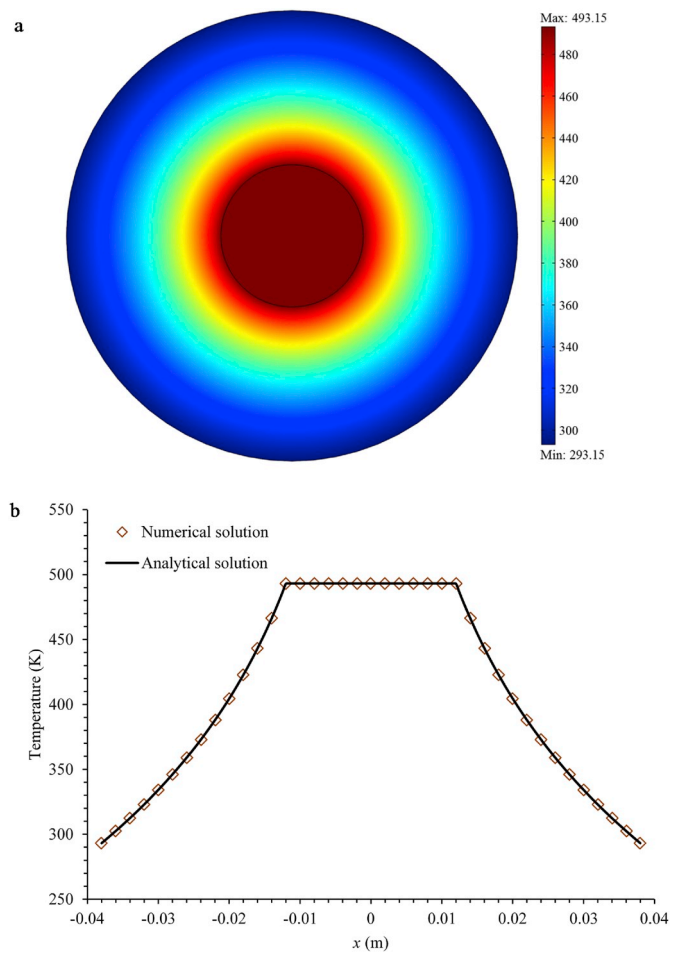


Fig. 7. Temperature distribution in two concentric cylinders: (a) Numerical result of temperature distribution in the concentric cylinder; (b) Numerical and analytical solutions of the temperature distribution the radius.

solution from the theory of elasticity for a hollow cylinder under internal hydrostatic pressure,<sup>39</sup> we obtain the following expressions:

$$\sigma_\rho = \frac{p}{\beta^2 - 1} \left( 1 - \frac{b^2}{\rho^2} \right) \quad (17)$$

$$\sigma_\phi = \frac{p}{\beta^2 - 1} \left( 1 + \frac{b^2}{\rho^2} \right) \quad (18)$$

where  $\beta = b/a$ .

The radial and circumferential deformations in the rock due to the radial pressure  $p$  are given by:

$$\varepsilon_{b\rho} = \frac{1}{E_b} (\sigma_\rho - \nu_b \sigma_\phi) = \frac{p}{E_b (\beta^2 - 1)} \left[ \left( 1 - \frac{b^2}{\rho^2} \right) - \nu_b \left( 1 + \frac{b^2}{\rho^2} \right) \right] \quad (19)$$

$$\varepsilon_{b\phi} = \frac{1}{E_b} (\sigma_\phi - \nu_b \sigma_\rho) = \frac{p}{E_b (\beta^2 - 1)} \left[ \left( 1 + \frac{b^2}{\rho^2} \right) - \nu_b \left( 1 - \frac{b^2}{\rho^2} \right) \right] \quad (20)$$

where  $E_b$  is elastic modulus and  $\nu_b$  is the Poisson's ratio of rock.

The circumferential deformation of is the sum of two contributions: the radial pressure due to thermal expansion as prompted by the temperature variation. As a consequence, the circumferential strain in the rock is expressed as:

$$\varepsilon_{b\phi}(\rho = a) = \frac{p}{E_b} \left( \frac{\beta^2 + 1}{\beta^2 - 1} + \nu_b \right) + \alpha_b \Delta T \quad (21)$$

**Table 1**  
Model parameters and boundary values for the numerical simulation.

Symbol	Value	Unit
Elastic modulus of core, $E_a$	42	GPa
Elastic modulus of rock, $E_b$	30	GPa
Poisson's ratio of core, $\nu_a$	0.33	-
Poisson's ratio of rock, $\nu_b$	0.2	-
Radius of core, $a$	12	mm
Radius of rock cylinder, $b$	38	mm
Thermal expansion coefficient of core, $\alpha_a$	15e-6	1/K
Thermal expansion coefficient of rock, $\alpha_b$	9e-6	1/K
Temperature of outer boundary of core, $T_a$	493.15	K
Temperature of outer boundary of rock, $T_b$	293.15	K

where  $\alpha_b$  is thermal expansion coefficient of rock.

The radial displacement,  $u$ , at any point in the core is:

$$u(\rho) = -\frac{(1-\nu_a)p}{E_a}\rho \quad (22)$$

where  $E_a$  is elastic modulus of the core and  $\nu_a$  is the Poisson's ratio of the core. The circumferential strain of the core due to the effect of the radial pressure  $p$ , is described by:

$$\varepsilon_{a\phi} = -\frac{(1-\nu_a)p}{E_a} \quad (23)$$

Similarly, the circumferential deformation of the core, at the core and rock interface due to the effect of the radial pressure and the temperature variation, is given by:

$$\varepsilon_{a\phi}(\rho=a) = \alpha_a \Delta T - \frac{(1-\nu_a)p}{E_a} \quad (24)$$

Using the compatibility equation linking the transverse deformations at the core and rock interface, the radial pressure is calculated as:

$$p = \frac{(\alpha_a - \alpha_b)\Delta T}{\frac{1}{E_b} \left( \frac{\beta^2+1}{\beta^2-1} + \nu_b \right) + \frac{1}{E_a} (1-\nu_a)} \quad (25)$$

Model parameters and boundary values for the numerical

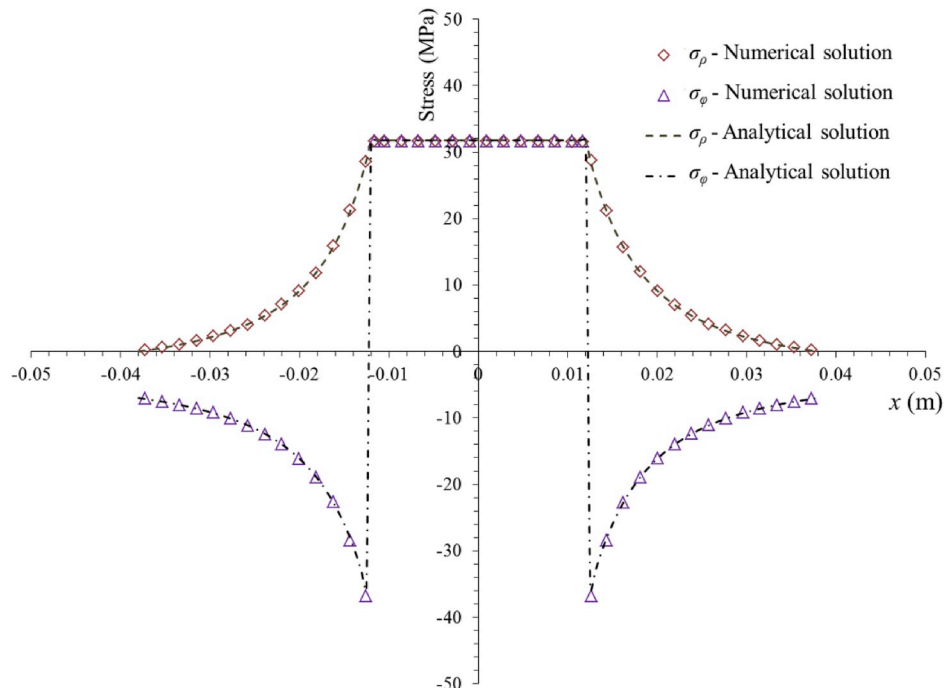
simulations are listed in Table 1. The final distribution of the temperature field acquired by the proposed TMD model is shown in Fig. 7. As illustrated in Fig. 7 (a), the inner cylindrical core has the maximum temperature ( $T_a = 493.15$  K), and from the boundary of the inner core to the outside, the temperature decreases gradually. The outer boundary of the rock cylinder has a minimum temperature ( $T_b = 293.15$  K). As shown in Fig. 7 (b), the numerical solution of the radial temperature distribution is in accordance with the analytical solution, validating the correctness of the proposed TMD model in simulating steady state heat conduction.

Fig. 8 shows the variation of radial stress and tangential stress along radial direction obtained from the proposed TMD model and analytic solutions. According to Eqs. (17) and (18), the internal boundary of the rock cylinder is subjected to constant stress. As a consequence, the data calculated by the proposed TMD model, as plotted by red diamonds and purple triangles in Fig. 8, remain constant in the range -12 mm-12 mm - the numerical solutions are consistent with the analytical solutions.

### 3.2. Validation against experimental observations

The experiments are carried out in the following steps. First, the rock specimens are heated to the designated temperature. Second, the temperature is retained constant for 2 h. Third, the rock specimens are allowed to cool naturally with the drop in temperature of the furnace. Finally, uniaxial compression tests are conducted. According to the experimental conditions,<sup>14</sup> a combined model, as shown in Fig. 9, is built to simulate the evolution of mechanical properties induced by thermal damage. Fig. 9 (a) shows the heat conduction model, which is used to simulate the temperature diffusion process. Fig. 9 (b) represents a model of a uniaxial compression test, which is used to examine the evolution of the stress-strain responses. In practice, numerical simulations are performed according to the experimental procedures to verify the evolution of the stress-strain curves against experimental results. Some of the thermal properties defining the of rock, which relate to thermal conduction, are missing in the experimental details<sup>14</sup> - we supplement these from typical magnitudes,<sup>40,41</sup> as listed in Table 2.

A comparison between the stress-strain curves for numerical and experimental results is shown in Figs. 10 and 11. The elastic modulus,



**Fig. 8.** Comparison of radial and tangential stress distributions between numerical and analytical solutions.

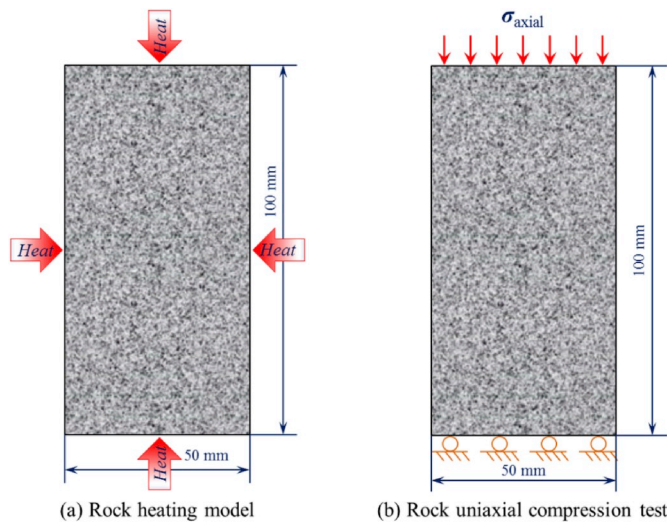


Fig. 9. Combined model for thermal-induced rock damage.

peak strength, peak strain, and porosity calculated by the proposed TMD model are consistent with the experimental results. With an increase in temperature, elastic modulus and strength of the rock decrease. Figs. 10 and 11 indicate that the influence of temperature on rock strength and porosity is relatively small when the heating retains the temperature to <200 °C. In particular, as can be seen from Fig. 10, the numerical results calculated by the dual-damage constitutive model are in good agreement with the experimental results.

4. Numerical analysis of thermal damage on rock mechanical behaviors

As noted above, the numerical simulations are conducted according to the experimental conditions. The heating rate is 30 °C/min with each designated temperature retained constant for 2 h. Then the temperature (power) is shut-off, the rock specimen is allowed to cool naturally with the cooling (temperature) of the furnace.<sup>14</sup> We follow the evolution of thermal damage, rock porosity and permeability in these experiments, specifically to define the failure patterns and mechanism of thermal damage.

4.1. Evolution of thermal damage

Thermally induced microcracks can significantly change the physical and mechanical properties of rock. From the numerical simulation, thermal-induced damage is shown in Fig. 12, which represents the evolution of rock damage induced by different heat treatments. As time progresses, the temperature of the rock gradually rises from the outside to the inside, congruent with the generation of damage. Apparent from Fig. 12 is that the higher the temperature the greater the rock damage – consequently reducing strength proportionately to the temperature - as shown in Fig. 10. Thus, it is confirmed from experimental observations and numerical results that rock damage occurs during thermal treatment, thus altering the mechanical properties and microstructure of the rock.

4.2. Evolution of porosity and permeability

Porosity and permeability are basic physical properties of rocks. In

Table 2  
Mechanical and thermal parameters for the numerical simulation.

Symbol	Value	Unit
Homogeneity index, <i>m</i>	10	–
Elastic modulus, <i>E</i>	37.6	GPa
Uniaxial compressive strength, UCS	183.2	MPa
Uniaxial tensile strength, $\sigma_t$	22.9	MPa
Density, $\rho$	2760	Kg/m <sup>3</sup>
Poisson ratio, $\nu$	0.25	–
Initial porosity, $\phi_0$	0.88	%
Initial permeability, $k_0$	$1.0 \times 10^{-19}$	m <sup>2</sup>
Initial thermal conductivity, $\lambda$	0.1	Wm <sup>-1</sup>
Initial specific heat capacity, <i>C</i>	700	J/(kg·K)
Thermal expansion coefficient, $\alpha_T$	$2.0 \times 10^{-6}$	1/K

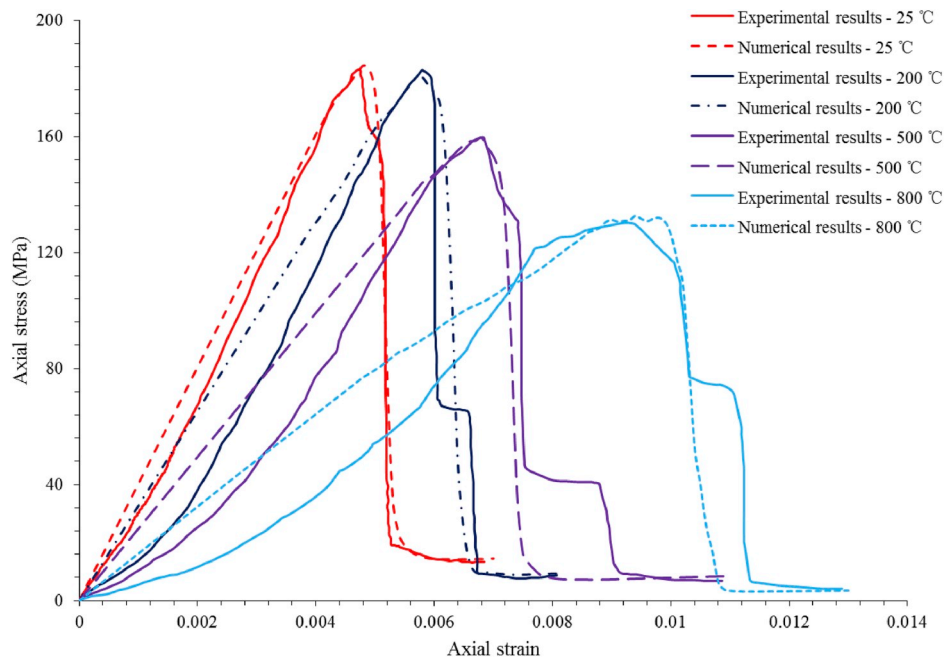


Fig. 10. Comparison between stress-strain curves recovered from numerical and experimental results.

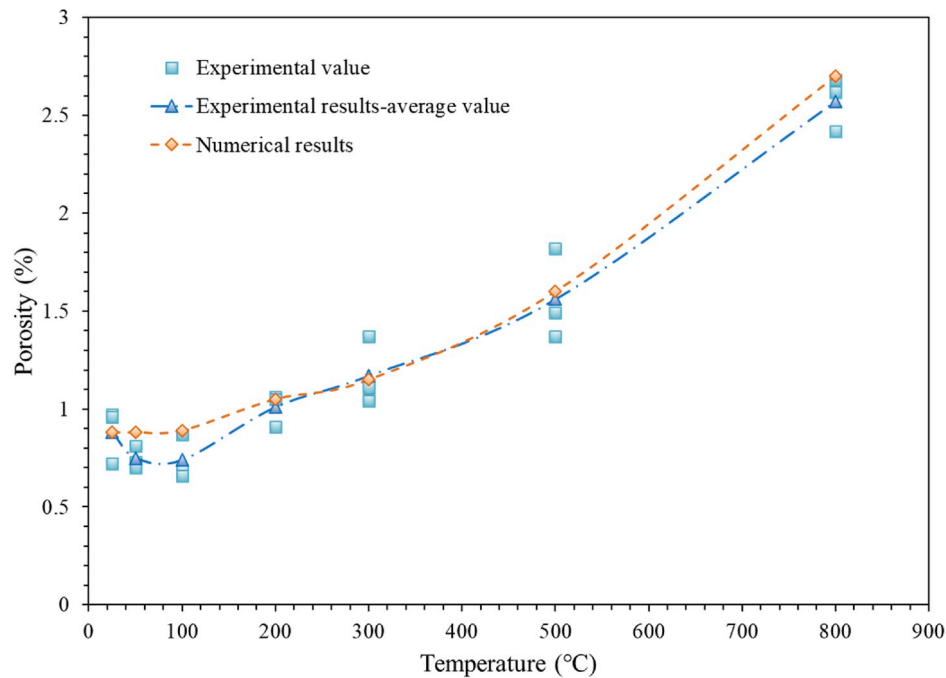


Fig. 11. Comparison between numerical results and experimental results for porosity change in granite subjected to different temperatures.

this study, the natural porosity of the rock ranges between 0.72% and 0.97%. As mentioned above, there are two stages in the thermal treatment. The rock is first heated to the designated temperature at a constant rate and then slowly cooled. We simulate the complete process of the heating and cooling treatment. Rock porosity and permeability are closely related to temperature change. As shown in Figs. 13 and 14, in the first stage, both porosity and permeability increase with temperature increase. In the second stage, as the temperature decreases, porosity and permeability decrease. The higher the temperature, the higher the porosity and permeability. However, the residual values of porosity and permeability remain larger than their initial values. That is, thermally-induced damage results in an irreversible increase in rock porosity and permeability, even though the temperature of the rock has been restored to its initial temperature. This is a result of remanent temperature-induced thermal damage that results either from the generation of new cracks or from the propagation of existing cracks.<sup>20</sup>

The data of Fig. 15 show the variation in permeability at eight different temperatures. Peak permeability represents rock permeability at the maximum temperature, when the volumetric strain is also the maximum. Residual permeability refers to the permeability when the temperature drops to the initial temperature. As shown in Fig. 15, both residual permeability and irreversible permeability increase with heat treatment temperature, a direct result of thermal damage. The higher the heat treatment temperature, the higher the residual permeability and irreversible permeability.

#### 4.3. Impact of thermal damage on rock failure patterns

Thermally-induced damage (as shown in Fig. 12) irreversibly changes the physical and mechanical properties of rock (as shown in Figs. 10, 11, 13, 14, and 15). The swelling/compaction in the rock due to its heterogeneous microstructure may be one mechanism of imparting the thermally-induced damage. According to experimental investigations on velocity and attenuation of ultrasonic waves<sup>8</sup> and acoustic emission (AE) monitoring,<sup>11,20</sup> thermal damage has a significant impact on microstructure and mechanical properties. Thermally-induced damage causes further alteration of the rock mass mechanical properties, resulting in a change in the failure patterns of

rock. This observation is illustrated in Fig. 16, where different thermal treatments correspond to different fracture patterns during failure. Numerical results confirm that the rearrangement of rock microstructure is induced by thermal damage. The damage processes and resulting failure geometries may be visualized by comparing the development of macro-scale fracturing with the distribution of tensile and shear cracking, as shown in Fig. 16.

#### 4.4. Mechanical mechanism of thermal damage

The damage variables of Eqs. (15) and (16) remain in the range from 0 to 1 regardless of the form or magnitude of damage. However negative and positive damage magnitudes are respectively adopted for damage in tension and in shear - merely to allow visualization of the two damage modes in the post-processed figures. In order to visualize these two damage modes, as can be seen in Figs. 12 and 16, the tensile damage is represented as negative ( $-1 \leq D < 0$ ), while the shear damage is represented as positive decimals ( $0 < D \leq 1$ ). During thermal treatment, the state of the microstructure of the rock mass is controlled by thermal expansion. As can be seen from Fig. 12, thermally-induced damage is dominated by tensile damage, since most values of the damage variable are negative. However, when the thermally treated rocks are simulated by the uniaxial compression model, some values of the damage variable could be positive, denoting shear failure, as shown in Fig. 16.

Fig. 17 shows the changes to the peak strength and peak strain with different levels of thermal treatment. It is clear that with the increase of temperature, the peak strength decreases and the peak strain increases. However, the change of the ratios of peak strength and peak strain are quite different, as shown in Table 3. When the temperature is 200 °C, the strength change ratio is -1.32%, and the elastic modulus change ratio is 20.83%. When the temperature is 500 °C, the strength change ratio is -12.98%, and the elastic modulus change ratio is -37.58%. At 800 °C, the strength change ratio is -28.25%, and elastic modulus change ratio is -63.16%. It is clear that the absolute value of the change ratio of the elastic modulus is larger than that of strength. Thus, the change ratios of the peak strength and elastic modulus are different, as illustrated in Fig. 18. Although this phenomenon has been reported in many experimental observations<sup>5,14,17,42,43</sup> the behavior has remained unexplained.

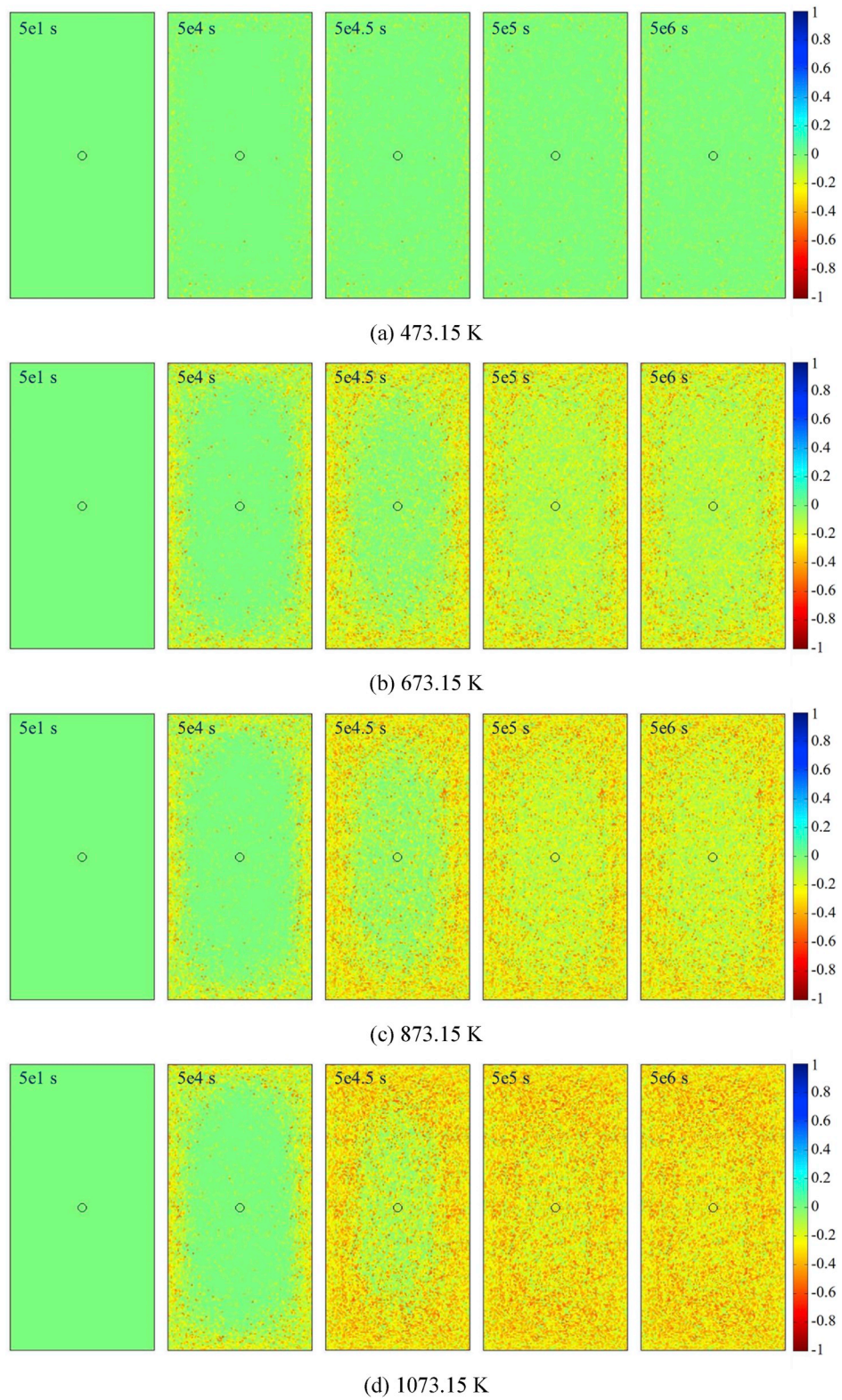


Fig. 12. Evolution of rock damage during thermal treatment.

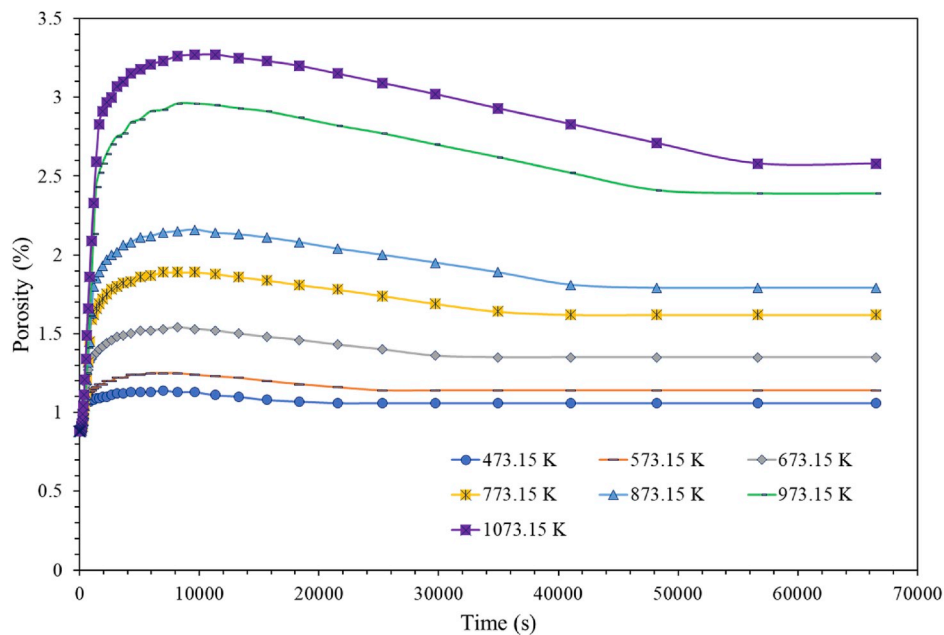


Fig. 13. Evolution of rock porosity during thermal treatment.

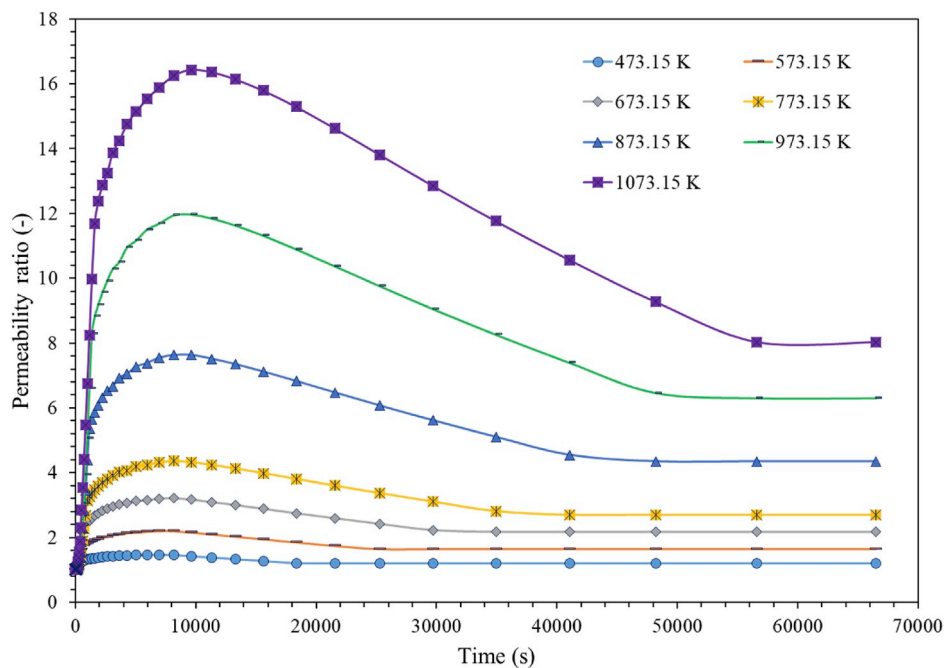


Fig. 14. Evolution of rock permeability during thermal treatment.

According to these experimental observations, in this study (Section 2), the TMD model is developed to explain the non-proportionality of these changes in peak strain and peak strength - based on the dual-damage constitutive theory. To summarize, the strength and elastic modulus of rock are subject to different damage mechanisms, represented by different damage laws.

5. Conclusions

This study develops a novel dual-damage constitutive model to examine coupled thermal-mechanical-damage process that result during thermal treatment. This approach accommodates damage variables to separately modify elastic modulus and strength and is applied to explain

the non-proportional alterations of elastic modulus and strength in heterogeneous rocks. The physical and mechanical processes involve fully coupling thermal transport in the porous rock to alterations in thermal conductivity and special heat capacity by simultaneously accommodating rock deformation and damage. Based on the results and the observations reported in previous studies, the following conclusions are drawn:

- (1) External heating raises the temperature of the rock from the outside to the inside with damage similarly propagating. Rock damage occurs during thermal treatment, thus altering the mechanical properties and the microstructure of the rock.

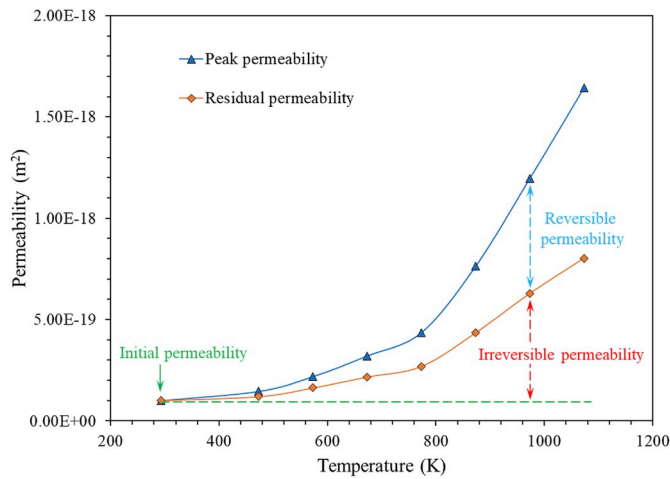


Fig. 15. Permeability evolution in rock subjected to different heat treatment temperatures.

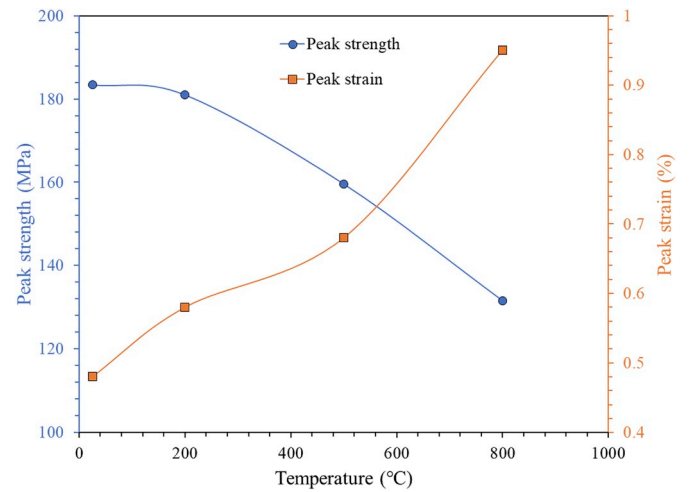


Fig. 17. Changes in peak strength and peak strain at different temperatures.

- (2) With an increase in temperature, both the elastic modulus and strength of the rock decrease. The higher the temperature, the lower the elastic modulus and strength. Numerical results are in good agreement with the experimental results.
- (3) Rock porosity and permeability are closely related to temperature change. Thermally-induced damage causes irreversible increases in rock porosity and permeability, even when the temperature of the rock is restored to its initial temperature.
- (4) Thermal treatment induces further alteration in the rock mass mechanical properties, reducing elastic modulus and weakening the rock, causing the rearrangement of rock microstructure and resulting in a change in the failure patterns of rock.
- (5) During thermal treatment, the state of the microstructure of the rock is controlled by thermal expansion. Numerical results demonstrate that thermally-induced damage is dominated by tensile damage.
- (6) With an increase of temperature, the peak strength decreases and the peak strain increases. However, the change ratios of peak strength and peak strain are quite different. The strength and elastic modulus of the rock conform to different damage laws. The proposed dual-damage constitutive model well explains the non-proportional alterations in peak strength and peak strain observed in many experiments.

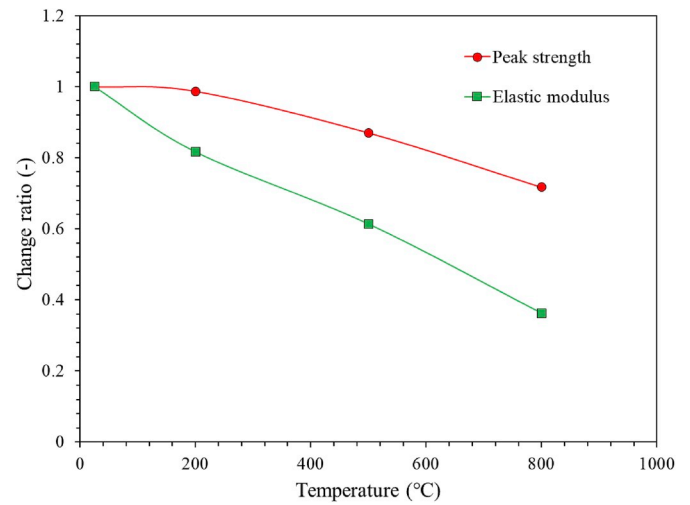


Fig. 18. Change ratios of peak strength and elastic modulus at different temperatures.

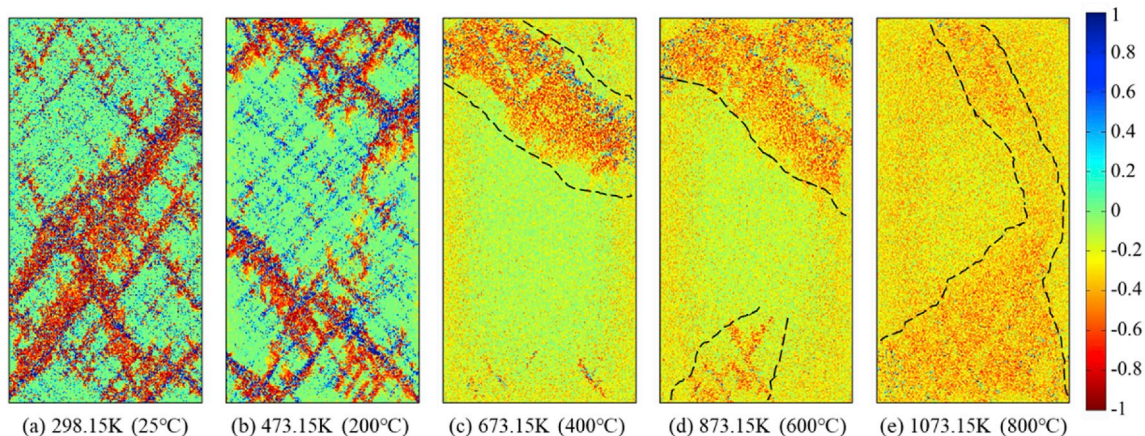


Fig. 16. Rock failure patterns following different thermal treatments.

**Table 3**

Variations in peak strength, elastic modulus, and peak strain at different temperatures.

$T_i$ , °C	25	200	500	800
$\Delta UCS/UCS$ , %	0	-1.32	-12.98	-28.25
$\Delta E/E$ , %	0	-17.02	-37.58	-63.16
$\Delta \epsilon_p/\epsilon_p$ , %	0	20.83	41.67	97.92

### Declaration of competing interest

The authors declared that they have no conflicts of interest to this work. We declare that we do not have any commercial or associative interest that represents a conflict of interest in connection with the work submitted.

### Acknowledgments

This work was funded by the National Key Research and Development Program of China (Grant No. 2016YFC0600801), National Science Foundation of China (Grant Nos. 51874014 and 51534002) and the Fundamental Research Funds for the Central Universities of China (Grant No. FRF-TP-19-027A1). These supports are gratefully acknowledged.

### Appendix A. Supplementary data

Supplementary data to this article can be found online at <https://doi.org/10.1016/j.ijrmms.2019.104185>.

### References

- 1 Tsang C-F. Linking thermal, hydrological, and mechanical processes in fractured rocks. *Annu Rev Earth Planet Sci.* 1999;27(1):359–384.
- 2 Shoko E, McLellan B, Dicks AL, da Costa JCD. Hydrogen from coal: production and utilisation technologies. *Int J Coal Geol.* 2006;65(3-4):213–222.
- 3 Heap MJ, Baud P, Meredith PG, Vinciguerra S, Bell AF, Main IG. Brittle creep in basalt and its application to time-dependent volcano deformation. *Earth Planet Sci Lett.* 2011;307(1):71–82.
- 4 Cai M, Brown ET. Challenges in the mining and utilization of deep mineral resources. *Engineering.* 2017;3(4):432–433.
- 5 Shao SS, Ranjith PG, Wasantha PLP, Chen BK. Experimental and numerical studies on the mechanical behaviour of Australian Strathbogie granite at high temperatures: an application to geothermal energy. *Geothermics.* 2015;54:96–108.
- 6 Darot M, Reuschlé T. Acoustic wave velocity and permeability evolution during pressure cycles on a thermally cracked granite. *Int J Rock Mech Min.* 2000;37(7):1019–1026.
- 7 Yavuz H, Demirdag S, Caran S. Thermal effect on the physical properties of carbonate rocks. *Int J Rock Mech Min Sci.* 2010;47(1):94–103.
- 8 Chaki S, Takarli M, Agbodjan WP. Influence of thermal damage on physical properties of a granite rock: porosity, permeability and ultrasonic wave evolutions. *Constr Build Mater.* 2008;22(7):1456–1461.
- 9 Heuze FE. High-temperature mechanical, physical and Thermal properties of granitic rocks—a review. *Int J Rock Mech Min Sci Geomech Abstr.* 1983;20(1):3–10.
- 10 Yang SQ, Ranjith PG, Jing HW, Tian WL, Ju Y. An experimental investigation on thermal damage and failure mechanical behavior of granite after exposure to different high temperature treatments. *Geothermics.* 2017;65:180–197.
- 11 Chen SW, Yang CH, Wang GB. Evolution of thermal damage and permeability of Beishan granite. *Appl Therm Eng.* 2017;110:1533–1542.
- 12 Heap MJ, Baud P, Meredith PG. Influence of temperature on brittle creep in sandstones. *Geophys Res Lett.* 2009;36.
- 13 Ranjith PG, Viete DR, Chen BJ, Perera MSA. Transformation plasticity and the effect of temperature on the mechanical behaviour of Hawkesbury sandstone at atmospheric pressure. *Eng Geol.* 2012;151:120–127.
- 14 Sun Q, Zhang W, Xue L, Zhang Z, Su TJES. *Thermal Damage Pattern and Thresholds of Granite.* vol. 74. 2015:2341–2349, 3.
- 15 Liang WG, Xu SG, Zhao YS, JRM, Engineering R. Experimental study of temperature effects on physical and mechanical. *Characteristics of Salt Rock.* 2006;39(5):469–482.
- 16 Tullis J, Yund RA. Experimental deformation of dry westerly granite. *J Geophys Res.* 1977;82(36):5705–5718.
- 17 Chen YL, Ni J, Shao W, Azzam R. Experimental study on the influence of temperature on the mechanical properties of granite under uni-axial compression and fatigue loading. *Int J Rock Mech Min Sci.* 2012;56:62–66.
- 18 Faoro I, Elsworth D, Candela T. Evolution of the transport properties of fractures subject to thermally and mechanically activated mineral alteration and redistribution. *Geofluids.* 2016;16(3):396–407.
- 19 Sun Q, Lu C, Cao LW, Li WC, Geng JS, Zhang WQ. Thermal properties of sandstone after treatment at high temperature. *Int J Rock Mech Min Sci.* 2016;85:60–66.
- 20 David C, Menéndez B, Darot M. Influence of stress-induced and thermal cracking on physical properties and microstructure of La Peyratte granite. *Int J Rock Mech Min Sci.* 1999;36(4):433–448.
- 21 Hueckel T, Peano A, Pellegrini R. A thermo-plastic constitutive law for brittle-plastic behavior of rocks at high temperatures. *Pure and Applied Geophysics PAGEOPH.* 1994;143(1-3):483–510.
- 22 Tang SB, Tang CA, Zhu WC, Wang SH, Yu QL. Numerical investigation on rock failure process induced by thermal stress. *Chin J Rock Mech Eng.* 2006;25(10):2071–2078.
- 23 Tang SB, Tang CA, Li LC, Liang ZZ. Numerical approach on the thermo-mechanical coupling of brittle material. *Chin J Comput Mech.* 2009;26(2):172–179.
- 24 Yu QL, Ranjith PG, Liu HY, et al. A mesostructure-based damage model for thermal cracking analysis and application in granite at elevated temperatures. *Rock Mech Rock Eng.* 2015;48(6):2263–2282.
- 25 Li LC, Yang TH, Tang CA, Huang XL, Li XB. Study on coupled thermal-mechanical-damage model in rock failure process. *Rock Soil Mech.* 2006;27(10):1727–1732.
- 26 Zhu WC, Liu LY, Liu JS, Wei CH, Peng Y. Impact of gas adsorption-induced coal damage on the evolution of coal permeability. *Int J Rock Mech Min Sci.* 2018;101:89–97.
- 27 Chilingar GV. Relationship between porosity, permeability, and grain-size distribution of sands and sandstones. In: van Straaten LMJU, ed. *Developments in Sedimentology.* vol. 1. Elsevier; 1964:71–75.
- 28 Kotyakhov FI. Interrelationship between major physical parameters of sandstones. *Neftyanoe Khozyaystvo.* 1949;12:29–32.
- 29 Ghassemi A. A review of some rock mechanics issues in geothermal reservoir development. *Geotech Geol Eng.* 2012;30(3):647–664.
- 30 Lan H, Martin CD, Andersson JC. Evolution of in situ rock mass damage induced by mechanical–thermal loading. *Rock Mech Rock Eng.* 2012;46(1):153–168.
- 31 Atkinson BK. Subcritical crack growth in geological materials. *J Geophys Res: Solid Earth.* 1984;89(B6):4077–4114.
- 32 Zhu WC, Tang CA. Micromechanical model for simulating the fracture process of rock. *Rock Mech Rock Eng.* 2004;37(1):25–56.
- 33 Liu LY, Li LC, Elsworth D, Zhi S, Yu YJ. The impact of oriented perforations on fracture propagation and complexity in hydraulic fracturing. *Processes.* 2018;6(11):213.
- 34 Liu LY, Zhu WC, Wei CH, Elsworth D, Wang JH. Microcrack-based geomechanical modeling of rock-gas interaction during supercritical CO<sub>2</sub> fracturing. *J Pet Sci Eng.* 2018;164:91–102.
- 35 Vosteen HD, Schellschmidt R. Influence of temperature on thermal conductivity, thermal capacity and thermal diffusivity for different types of rock. *Phys Chem Earth.* 2003;28(9-11):499–509.
- 36 Li LC, Tang CA, Wang SY, Yu J. A coupled thermo-hydrologic-mechanical damage model and associated application in a stability analysis on a rock pillar. *Tunn Undergr Space Technol.* 2013;34(1):38–53.
- 37 Abdalla H. Concrete cover requirements for FRP reinforced members in hot climates. *Compos Struct.* 2006;73(1):61–69.
- 38 Masmoudi R, Zaidi A, Gerard P. Transverse thermal expansion of FRP bars embedded in concrete. *J Compos Constr.* 2005;9(5):377–387.
- 39 Timoshenko S, Goodier JN. *Theory of Elasticity.* New York: McGraw-Hill; 1970.
- 40 Yan CZ, Zheng H. A coupled thermo-mechanical model based on the combined finite-discrete element method for simulating thermal cracking of rock. *Int J Rock Mech Min Sci.* 2017;91:170–178.
- 41 Tang SB, Zhang H, Tang CA, Liu HY. Numerical model for the cracking behavior of heterogeneous brittle solids subjected to thermal shock. *Int J Solids Struct.* 2016;80:520–531.
- 42 Xu XL, Kang ZX, Ji M, Ge WX, Chen J. Research of microcosmic mechanism of brittle-plastic transition for granite under high temperature. *Procedia Earth and Planetary Science.* 2009;1(1):432–437.
- 43 Liu S, Xu JY. An experimental study on the physico-mechanical properties of two post-high-temperature rocks. *Eng Geol.* 2015;185:63–70.